molecular pharmaceutics

Article

Cite This: Mol. Pharmaceutics 2019, 16, 1498−1506

pubs.acs.org/molecularpharmaceutics

Voxel-Based Dosimetry of Iron Oxide Nanoparticle-Conjugated ^{177}Lu-Labeled Folic Acid Using SPECT/CT Imaging of Mice

Arun Gupta,[†,▽] Jae H. Shin,[‡,▽] Min S. Lee,[†,§] Ji Y. Park,[†] Kyuwan Kim,[†] Joong H. Kim,[∥] Minseok Suh,[†] Cho R. Park,[†] Young J. Kim,[†] Myung G. Song,[†] Jae M. Jeong,[†] Dong S. Lee,[†,⊥] Yun-Sang Lee,[*,†] and Jae S. Lee[*,†,§,#]

[†]Department of Nuclear Medicine, Seoul National University College of Medicine, Seoul 03080, Korea

[‡]Department of Chemistry, Graduate School, Kyung Hee University, Seoul 02447, Korea

[§]Interdisciplinary Program in Radiation Applied Life Science, Seoul National University, Seoul 08826, Korea

[∥]Center for Ionizing Radiation, Korea Research Institute of Standards and Science, Daejeon 34113, Korea

[⊥]Department of Molecular Medicine and Biopharmaceutical Sciences, Graduate School of Convergence Science and Technology, Seoul National University, Suwon 08826, Korea

[#]Department of Biomedical Sciences, Seoul National University College of Medicine, Seoul 03080, Korea

ABSTRACT: Several radiolabeled folic acid conjugates have been developed for targeted imaging and therapy. However, the therapeutic concept with radiolabeled folate conjugates has not yet been applied to clinical applications owing to the high renal absorbed dose. The effectiveness of targeted radionuclide therapy (TRT) depends primarily on the absorbed dose rate and on the total absorbed dose delivered to the tumor and to normal tissue. Owing to various limitations associated with organ level dosimetry, voxel-based dosimetry has become essential for the assessment of a more accurate absorbed dose during TRT. In this study, we synthesized iron oxide nanoparticle (IONP)-conjugated radiolabeled folate (^{177}Lu-IONP-Folate) and performed voxel-based dosimetry using SPECT/CT images of normal mice through direct Geant4 application for emission tomography (GATE) Monte Carlo (MC) simulation. We also prepared ^{177}Lu-Folate and ^{177}Lu-IONPs for the comparison of absorbed doses with that of ^{177}Lu-IONP-Folate. In addition, we calculated the mean absorbed dose at the organ-level using the medical internal radiation dose (MIRD) schema. The radioactivities of all three radiotracers were mainly accumulated in the liver and kidneys immediately after injection. For the kidneys, the voxel-based absorbed doses obtained with ^{177}Lu-IONP-Folate, ^{177}Lu-Folate, and ^{177}Lu-IONPs were 1.01 ± 0.17, 2.46 ± 0.50, and 0.52 ± 0.08 Gy/MBq, respectively. The renal absorbed dose decreased significantly (~half) when ^{177}Lu-IONP-Folate was used compared with when the ^{177}Lu-Folate only was used. The mean absorbed dose values obtained at organ-level using the MIRD schema were comparable to voxel-based absorbed doses estimated with GATE MC. The voxel-based absorbed dose values obtained in this study of individualized activity show that the renal absorbed dose could be reduced to almost half with ^{177}Lu-IONP-Folate. Therefore, ^{177}Lu-IONP-Folate could be clinically applicable in the TRT of folate receptor-positive cancers in a personalized manner when using the voxel-based dosimetry method.

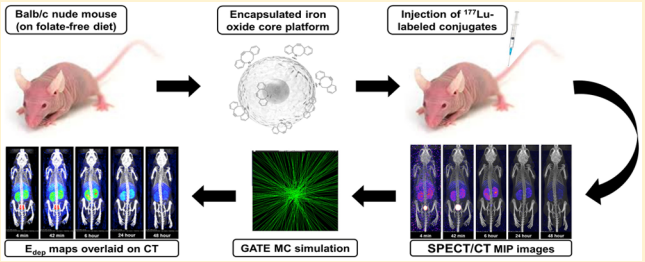

KEYWORDS: *SPECT/CT, folate, IONPs, voxel-based, absorbed dose, GATE, MIRD*

INTRODUCTION

Small animal single photon emission computed tomography (SPECT) plays a fundamental role in preclinical targeted radionuclide therapy (TRT) using theranostic radionuclides (e.g., ^{131}I, ^{188}Re, and ^{177}Lu) for new radiopharmaceutical development because of the translation of results from preclinical to clinical settings.[1,2] Moreover, the computed tomography (CT)-based attenuation correction and anatomic information obtained from integrated SPECT/CT systems have increased the accuracy of SPECT image quantification.[3] TRT, and especially peptide receptor radionuclide therapy (PRRT), has gained increasing importance for the treatment of various cancers, including lymphoma, glioblastoma, neuroendocrine tumors, and prostate cancer.[4,5] For successful TRT, selective concentration and prolonged retention of the radiopharmaceutical within the tumor is required to achieve the best therapeutic effect, while minimizing toxicity to surrounding normal tissues.[6] Peptide analogs, such as RGD (arginylglycylaspartic acid), GRP (gastrin-releasing peptide),

Received: October 29, 2018
Revised: February 15, 2019
Accepted: March 1, 2019
Published: March 1, 2019

DOI: 10.1021/acs.molpharmaceut.8b01125
Mol. Pharmaceutics 2019, 16, 1498−1506

octreotide, and folate, are conjugated with suitable radionuclides to target specific receptors overexpressed in a particular cancer type.[7,8] Folate receptors (FRs) are membrane bound glycoproteins that are highly expressed in many human malignancies, such as ovarian, cervical, renal, lung, and breast carcinomas; however, there are very limited expressions of these receptors in normal organs and tissues.[9,10]

Folic acid conjugated with theranostic radionuclides has been used as a valuable tool to implement novel and effective anticancer therapies.[9] For example, ^{177}Lu has several advantages, (i) it emits low-energy (0.5 MeV) beta particles that show efficient crossfire effects in cancer cells; (ii) it has a favorable half-life of 6.7 days; and (iii) it has gamma emissions with adequate energies (208.4, 112.9, and 56.30 keV) to perform SPECT imaging.[11] Despite the excellent tumor targeting ability of ^{177}Lu-labeled folic acid conjugates, a substantial fraction of radioactivity is always found in the kidneys, owing to the presence of FRs in the proximal tubule cells.[12,13] Hence, there is always a risk of radiation-induced nephropathy to the radiosensitive kidneys by particle emitting radioisotopes. Such a high kidney uptake necessitates the reduction in dosage of radiolabeled folate to be administered during targeted therapy. Consequently, the radiation energy absorbed in cancer cells cannot be sufficient for complete remission. Folate-based radiopharmaceuticals with prolonged blood circulation time could improve this situation. Muller et al.[9] synthesized a radiolabeled folate conjugate with an albumin binding entity for folic acid-targeted radionuclide therapy in mice that resulted in a significant increase in the tumor-to-kidney uptake ratio.

During PRRT, the absorbed dose must be determined as accurately as possible to obtain appropriate absorbed dose–response relationships.[14] Absorbed doses in small animals can be measured using the medical internal radiation dose (MIRD) formalism that uses organ *S*-values (mean absorbed dose in a target organ per radioactivity decay in a source organ).[15] However, the mean absorbed estimated at organ level using the MIRD approach does not incorporate patient- or animal-specific activity distributions and geometries because it assumes homogeneous activity distributions in organs and a generalized anatomy.[16,17] Meanwhile voxel-based dosimetry, using Monte Carlo (MC) simulation, is regarded to produce more realistic and high precision dose distribution in organs at the voxel-level since it considers tissue heterogeneity and the true activity distribution in the whole body. As therapeutic efficacy and normal tissue toxicity are of great concern, and because there is much less tolerance for inaccuracies in dosimetry during TRT, voxel-based dosimetry is necessary.[18]

Many researchers have addressed the limitations associated with organ-based dosimetry methods; on this basis, voxel-based personalized dosimetry has been implemented to estimate more accurate absorbed doses in sensitive organs.[19] Above all, SPECT/CT-based individualized dosimetry may be crucial where the average absorbed dose to an organ does not provide the information required to predict the potential biologic effects.[20] The voxel-based absorbed dose estimated using the MC approach considers both inhomogeneous activity distribution and medium heterogeneity present within a mouse's body.[21]

In this study, we synthesized ^{177}Lu-labeled folate radiopharmaceutical conjugated with iron oxide nanoparticles (IONPs) (^{177}Lu-IONP-Folate) with the aim of improving the overall tissue distribution and reducing the renal absorbed dose. We compared the biodistribution and absorbed dose, calculated using SPECT image voxel-based dosimetry through direct MC simulation, of ^{177}Lu-IONP-Folate, ^{177}Lu-Folate, and ^{177}Lu-IONPs in normal mice. We also acquired SPECT/CT images of KB tumor bearing mice using ^{177}Lu-IONP-Folate, ^{177}Lu-Folate, and ^{177}Lu-IONPs and performed voxel-based dosimetry to compare the binding affinity of the prepared ^{177}Lu-labeled folate conjugates.

MATERIALS AND METHODS

General. IONPs (5 nm) in nonpolar solvent (chloroform) were provided by the School of Advanced Materials Engineering, Kookmin University. DSPE-PEG (2000)-DBCO was purchased from Avanti Polar Lipids, Inc. (Ala, USA). NOTA-DBCO and NOTA-PEG$_3$-N$_3$ were purchased from FutureChem CO., Ltd. (Seoul, Korea). All other reagents and solvents were purchased from Sigma-Aldrich (MO, USA). The hydrodynamic diameter and size distribution of nanoparticles were analyzed by a dynamic light scattering (DLS) system, Zetasizer Nano ZS90 (Malvern Instruments Ltd., Worcestershire, UK), and a JEM-1010 transmission electron microscope (TEM; JEOL, Tokyo, Japan). The ^{177}LuCl$_3$ was purchased from ITG GmbH (Munich, Germany). Instant thin layer chromatography-silica gel (ITLC-SG) plates were obtained from Agilent Technologies, Inc. (CA, USA). In addition, radio-thin layer chromatography (radio TLC) was performed with a Bio-Scan AR-2000 System imaging scanner (Bioscan, WI, USA). Radioactivity was measured by a gamma scintillation counter (Packard Cobra II, GMI, NM, USA). All the animal studies were approved by the Institutional Animal Care and Use Committee (IACUC) of Seoul National University Hospital, Seoul, Korea. SPECT/CT imaging of mice was performed using a four-headed NanoSPECT/CT (Bioscan Inc.) scanner with multipinhole collimators. All acquired SPECT data were iteratively reconstructed using the ordered subset expectation maximization (OSEM) reconstruction algorithm of the HiSPECT NG software (Scivis GmbH, Germany).

Preparation of Clickable IONPs (IONP-DBCOs). Clickable IONPs (IONP-DBCOs) were prepared by the previously reported method with little modification.[22] Polysorbate 60 solution at a concentration of 10% (v/v) in distilled water (10 mL) was added to DSPE-PEG (2000)-DBCO (dibenzocyclooctyne, 123 mg). The mixture was sonicated at 30 °C for 30 min. To this micelle mixture (1.5 mL) in a 20 mL glass vial, 100 μL of IONP solution (50 mg/mL in $CHCl_3$) was added, and the mixture containing $CHCl_3$ was evaporated using a rotary evaporator. After sonication for 1 h, the reaction mixture was centrifuged and purified at 40 000 rpm and 4 °C for 2 h using OptiPrepTM gradients. After purification, the gradient was removed by an Amicon filter (Amicon Ultra-0.5, 100 kDa, Merck Millipore, 10000 rpm, 25 °C, 2 min).

Preparation of ^{177}Lu-NOTA-DBCO or -N$_3$. The ^{177}LuCl$_3$ (148 MBq, 4 μL) was added to 160 μL of 1 M sodium acetate buffer (pH 5.6), followed by the addition of NOTA-DBCO or NOTA-PEG$_3$-N$_3$ (1.34 μL, 2 nmol, 1 mg/mL in water). The mixture was incubated at 70 °C for 10 min to give ^{177}Lu-NOTA-DBCO or -N$_3$, which was used for the labeling of Folate-N$_3$, IONP-DBCO, or IONP-Folate-DBCO without further purification.

Preparation of ^{177}Lu-Folate, ^{177}Lu-IONPs, and ^{177}Lu-IONP-Folate. The ^{177}Lu-Folate was prepared by adding 264 μL of

DOI: 10.1021/acs.molpharmaceut.8b01125
Mol. Pharmaceutics 2019, 16, 1498–1506

Folate-N_3 (80 μg, 8 nmol) in sodium ascorbate solution (300 μg/mL) to the 148 MBq of ^{177}Lu-NOTA-DBCO solution (165.34 μL, 2 nmol) and vortexed at 38 °C for 1 h.

The ^{177}Lu-IONP was prepared by adding IONP-DBCO (1.2 mg, 8 nmol) to the 148 MBq of ^{177}Lu-NOTA-N_3 solution (165.34 μL, 2 nmol) and vortexed at 38 °C for 1 h.

To the IONP-DBCO (1.2 mg, 8 nmol) solution in distilled water (10 mL), 33 μL of Folate-N_3 (10 μg, 1 nmol) in sodium ascorbate solution (300 μg/mL) was added and kept at 38 °C for 15 min. The reaction mixture was purified using a desalting column (PD-10, GE Healthcare, WI, USA) and concentrated to 100 μL using an Amicon filter. IONP-Folate-DBCO (100 μL, 8 nmol) was added to the 148 MBq of ^{177}Lu-NOTA-N_3 solution (165.34 μL, 2 nmol) and vortexed at 38 °C for 1 h to prepare the ^{177}Lu-IONP-Folate.

Animal Preparation. Specific pathogen-free 4-week old male BALB/c nude mice were used in this study. Since a normal rodent diet contains a high level of folate, the mice received a folate-free diet (A08112101, Research Diets Inc., New Brunswick, NJ, USA) for at least 3 weeks to reduce serum folate level to a physiologic range. We prepared three groups of normal and three groups of KB tumor bearing mice (5 mice in each group) for SPECT/CT imaging with three different ^{177}Lu-labled radiotracers (^{177}Lu-Folate, ^{177}Lu-IONPs, and ^{177}Lu-IONP-Folate).

Tumor Mouse Model. KB cells were obtained from the Korea Cell Line Bank (Seoul, Korea). Cells were cultured in RPMI 1640 medium containing 10% (v/v) fetal bovine serum and 1% Anti-Anti (Gibco by Life Technologies, CA, USA) in a 5% CO_2-humidified incubator at 37 °C, except KB cells were cultured in folate deficient RPMI but were otherwise identical. Specific pathogen-free 4-week old male BALB/c nude mice were purchased for the preparation of KB tumor bearing mice. After 3 weeks of the folate-free diet, FR-positive KB cells (1 × 106 cells) were inoculated subcutaneously into the leg of each mouse.

In Vitro Cell Binding Affinity. In vitro cell binding affinity of ^{177}Lu-Folate and ^{177}Lu-IONP-Folate were measured by the previously reported method with little modifications.[23] In brief, FR-positive KB cells (human cervical carcinoma) were obtained from the Korean Cell Line Bank (Seoul, Korea). The medium in each well was then replaced with fresh medium containing increasing concentrations of ^{177}Lu-Folate (1.34 nM) or ^{177}Lu-IONP-Folate (0.03−3.33 nM) in the presence or absence of a 200-fold molar excess of free folate. The binding affinity was calculated using GraphPad Prism 5 (GraphPad Software Inc., San Diego, CA, USA).

SPECT/CT Imaging. We acquired whole-body SPECT/CT imaging for the first group of normal mice via tail vein injection of ^{177}Lu-Folate (11.99 ± 1.57 MBq). Similarly, we acquired SPECT/CT imaging of the second and third groups of normal mice after the injection of ^{177}Lu-IONPs (9.16 ± 1.21 MBq) and ^{177}Lu-IONP-Folate (5.50 ± 0.10 MBq), respectively. We acquired six sequential SPECT scans at 4, 12, 18, 24, 31, and 42 min after each radiotracer injection (5−15 s per frame), followed by a CT scan without moving the mouse from the imaging table. We further acquired a SPECT/CT of mice at 6 (30 s per frame), 24 (45 s per frame), and 48 h (60 s per frame) after radiotracer injection. SPECT scans were acquired with 40 projections (frames) at an 18° angular step. The energy peaks of ^{177}Lu were set to 56.1 keV ± 10%, 112.9 keV ± 10%, and 208.4 keV ± 10%. The CT acquisition was performed to correct for gamma ray attenuation and to obtain anatomical information using a 55 mA tube current and 145 kVp. We also acquired SPECT/CT images of each group of KB tumor bearing mice after tail vein injection of ^{177}Lu-Folate (11.82 ± 0.72 MBq), ^{177}Lu-IONPs (13.50 ± 0.61 MBq), and ^{177}Lu-IONP-Folate (16.58 ± 0.32 MBq). We used the same imaging protocol and image reconstruction algorithms which were applied for SPECT/CT imaging of normal mice. Before conducting animal imaging, we performed phantom studies to evaluate the performance parameters and quantitative accuracy of the NanoSPECT/CT scanner for ^{177}Lu mouse imaging.[24]

Image Reconstruction. The reconstructed SPECT images had a matrix size of 80 × 80 × 222 and a voxel size of 0.45 × 0.45 × 0.45 mm^3. The CT projection data were reconstructed (real-time) using a cone-beam-filtered back projection with a matrix size of 204 × 204 × 632 and a voxel size of 0.15 × 0.15 × 0.15 mm^3. The reconstructed SPECT and CT images were analyzed using InVivoScope software provided by the NanoSPECT/CT system for coregistration and MIP (maximum intensity projection) image generation. The CT and SPECT DICOM images were then post processed using the AMIDE tool to match the voxel size for MC simulation. The voxel intensity of SPECT images was given in counts, which was converted to activity (Bq) using the calibration factor of ^{177}Lu measured for the NanoSPECT/CT scanner before mice imaging.[24]

SPECT Image-Based Biodistribution of Radiotracers. The volumes of interest (VOIs) were manually drawn over the major organs (brain, heart, lungs, liver, kidneys, and tumor) on CT images of mice acquired at different time points. The regions of interest (ROIs) were drawn carefully over the organs on every slice to maintain the consistency in the size and shape of VOIs obtained at each time points. The number of voxels within the VOIs drawn for an organ at each time point were averaged and multiplied by voxel volume and tissue density[25] to estimate the organ mass.

The activity uptakes in the organs from ^{177}Lu-Folate, ^{177}Lu-IONPs, and ^{177}Lu-IONP-Folate were estimated by applying the VOIs (drawn on CT images) over the organs on respective SPECT images acquired at different time points. The activity (Bq) measured in the organ was normalized to the total injected dose of each radiotracer and divided by the mass of respective organs to obtain the percentage of injected dose per gram (%ID/g). The SPECT image-based biodistribution was plotted as a function of time to generate time activity curves (TACs) of organs for all three radiotracers. The time-integrated activity ($\tilde{A}$) in the organs were estimated for these radiotracers using the trapezoidal sum of area under curves (AUCs) of the TACs using eq 1, where A_0 is the initial injected activity of radiotracer, and $A(t)$ is the activity of each organ at time t. $\tilde{A}$ was extrapolated to infinity using the integral of physical decay for the curve tail at the end of the scan

$$\tilde{A} = \int_0^\infty A(t)dt = \int_0^\infty A_0 \exp\left(-\frac{\ln(2)}{T_{1/2}}t\right)dt \quad (1)$$

GATE MC Simulation Set Up. GATE v.7.0 was used for the simulations to estimate the voxel-based absorbed doses in the organs of mice. The simulation was conducted in an in-house computing cluster with a 60-core CPU and 80 GB of RAM. The CT and SPECT images of real mice that were modified to have the same voxel dimension (0.45 × 0.45 × 0.45 mm^3) were used as the voxelized phantom and voxelized

DOI: 10.1021/acs.molpharmaceut.8b01125
Mol. Pharmaceutics 2019, 16, 1498−1506

source, respectively, in the inputs for GATE MC. The ^{177}Lu ion source type of Geant4 v.9.6.3 was used for the simulation. GATE's standard electromagnetic physics package, which includes the photoelectric effect, Compton, bremsstrahlung, and positron-electron annihilation, was used during all simulations. No energy cuts or variance reduction techniques were applied in the physical processes. GATE was run with a Mersenne Twister random number generator.[26] A separate simulation for each SPECT image was run with corresponding biodistribution and scan duration. We ran simulations for 1/10th to 1/100th of the SPECT scan duration to reduce the simulation time and extensive computational cost. However, the statistical uncertainties were kept below 2% at the voxel level.

Voxel-Based Dosimetry Using the Direct MC Method. GATE MC is provided with a mechanism, named DoseActor, that stores the absorbed dose in a given volume in a 3D matrix.[27] The output of GATE MC simulation provides an energy deposition (E_{dep}) map, dose distribution map, and the local statistical uncertainty. By using the DoseActor mechanism, deposited energy (J) in each organ was extracted from all nine E_{dep} maps of a mouse using VOIs previously drawn on CT images. The absorbed dose (Gy) in the organs at the voxel level was subsequently calculated from deposited energy in the organs, which was further divided with respective simulation time to obtain dose rate (Gy/h) in a given organ. The dose rate vs time curves were plotted until 48 h and extrapolated to infinity to measure the total voxel-based absorbed dose in the organs received by ^{177}Lu-Folate, ^{177}Lu-IONPs, and ^{177}Lu-IONP-Folate. The steps followed for the absorbed dose estimation using direct GATE MC simulation are illustrated in Figure 1. The voxel-based absorbed doses measured in the organs were normalized to the injected activity of radiotracers in each mouse image and presented as Gy/MBq.

Absorbed Dose Estimation at the Organ Level Using the MIRD Schema. Using the MIRD formalism, we also calculated the absorbed dose at organ level using published *S*-values and the time-integrated activity ($\tilde{A}$) obtained from the SPECT image-based biodistribution data of ^{177}Lu-Folate, ^{177}Lu-IONPs, and ^{177}Lu-IONP-Folate. The mean absorbed dose (D) in the target organ (r_t) was calculated using the time-integrated activity ($\tilde{A}$) in the source organ (r_s) and the *S*-value [$S(r_t \leftarrow r_s)$] given by eq 2

$$D(r_t \leftarrow r_s) = \tilde{A} \times S(r_t \leftarrow r_s) \quad (2)$$

The *S*-values for the source-target organ pair were used from the database published by Larsson et al.[28] They estimated mouse *S*-values of ^{177}Lu were from MOBY phantom using EGS4 and MCNPX code. Organ mass correction was performed while using *S*-values in the MIRD formalism. We compared the voxel-based absorbed dose in the organs received by all three radiotracers with the mean absorbed dose values obtained using the MIRD schema.

RESULTS

Characteristics of ^{177}Lu-Labeled Conjugates. The hydrodynamic size of IONP-DBCO was 11.4 nm, and the zeta potential was −9.6 mV. The binding affinity (K_d) of ^{177}Lu-folate and ^{177}Lu-IONP-folate were 52.74 ± 8.26 and 10.68 ± 2.53 nM, respectively. After ^{177}Lu labeling, there were no significant size changes from IONP-DBCO. The radiolabeling efficiency (LE = 99%) was determined using ITLC after a

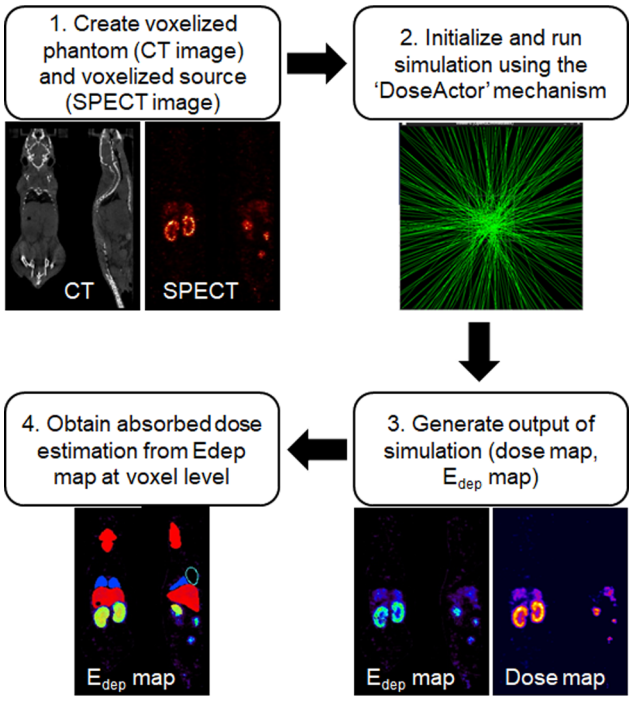

Figure 1. Methods applied to estimate the absorbed dose at the voxel level using GATE MC simulation. VOIs drawn over the organs on CT images were transferred to the E_{dep} maps for the calculation of the absorbed dose (step 4). CT, computed tomography; E_{dep}, energy deposition; GATE, Geant4 application for emission tomography; MC: Monte Carlo; and SPECT, single photon emission computed tomography.

radiolabeling procedure with 0.1 M citric acid as the mobile phase. The R_f of ^{177}Lu-NOTA-PEG$_3$-N$_3$ or ^{177}Lu-NOTA-ADIBO was 0.5−0.6; the R_f of the free radioisotope was 0.9−1.0. The LEs of ^{177}Lu-Folate, ^{177}Lu-IONPs, and ^{177}Lu-IONP-Folate were 99%, and the R_f of all the radiotracers was 0.2−0.3.

SPECT Image-Based Biodistribution. The TACs of blood, liver, and kidneys of normal mice for ^{177}Lu-Folate, ^{177}Lu-IONPs, and ^{177}Lu-IONP-Folate are shown in Figure 2. The highest accumulation of ^{177}Lu-labeled conjugates was found in the kidneys. The peak uptakes of ^{177}Lu-Folate, ^{177}Lu-IONPs, and ^{177}Lu-IONP-Folate in the kidneys were observed within 1 h after injections and were 38.78 ± 5.70, 25.46 ± 1.6, and 29.95 ± 6.13 %ID/g, respectively (Figure 2A). Rapid decline of renal uptake was observed with the IONPs based ^{177}Lu-labeled folate conjugate, while ^{177}Lu-Folate showed prolonged uptake in the kidneys. Uptakes in the kidneys after 48 h were 11.22 ± 1.71, 1.97 ± 0.27, and 3.29 ± 0.56 for ^{177}Lu-Folate, ^{177}Lu-IONPs, and ^{177}Lu-IONP-Folate, respectively. The peak uptake of ^{177}Lu-Folate in the liver was 8.50 ± 1.43 %ID/g; however, ^{177}Lu-IONPs and ^{177}Lu-IONP-Folate showed a higher peak uptake in the liver (11.73 ± 1.68 and 10.32 ± 0.91 %ID/g, respectively; Figure 2B). The uptake of ^{177}Lu-IONPs and ^{177}Lu-IONP-Folate in the liver remained higher than that of ^{177}Lu-Folate. After 48 h, the uptakes in the liver were 3.95 ± 0.28 (^{177}Lu-Folate), 6.10 ± 1.10 (^{177}Lu-IONPs), and 4.98 ± 0.17 %ID/g (^{177}Lu-IONP-Folate). As shown in Figure 2C, ^{177}Lu-IONP-Folate was retained in the blood for relatively longer than ^{177}Lu-Folate. The radioactivities of ^{177}Lu-Folate, ^{177}Lu-IONPs, and ^{177}Lu-IONP-Folate in the blood 48 h after injection were 0.54 ± 0.02, 0.50 ± 0.04, and 0.98 ± 0.11 %ID/g, respectively. Similar biodistribution of

DOI: 10.1021/acs.molpharmaceut.8b01125
Mol. Pharmaceutics 2019, 16, 1498−1506

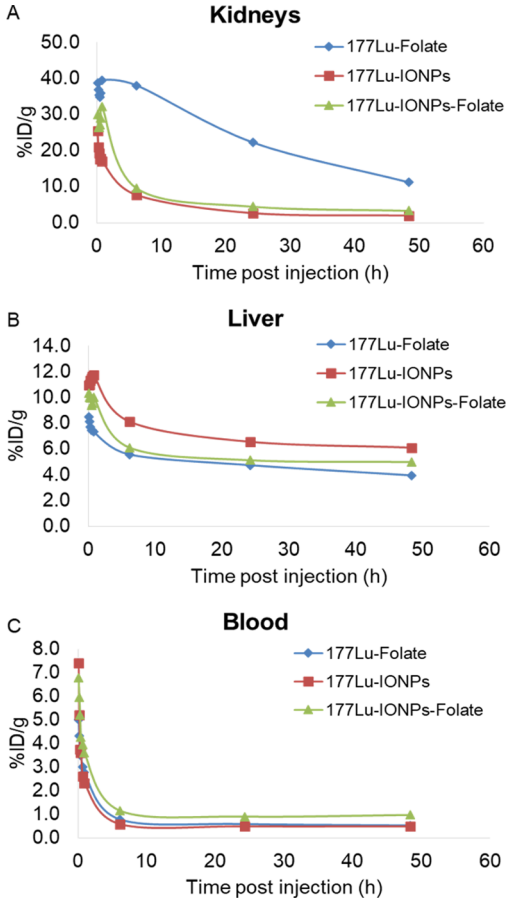

Figure 2. Percentage of injected dose per gram (%ID/g, mean, $n = 5$) as a function of time (corrected for radiation decay) obtained with ^{177}Lu-Folate, ^{177}Lu-IONPs, and ^{177}Lu-IONP-Folate in normal mice for (A) kidneys, (B) liver, and (C) blood. IONPs, iron oxide nanoparticles.

radioactivities in the organs were observed when TACs of ^{177}Lu-Folate, ^{177}Lu-IONPs, and ^{177}Lu-IONP-Folate were plotted for KB tumor bearing mice. We found that the uptake of ^{177}Lu-IONP-Folate in the tumors was increased compared to the uptakes of ^{177}Lu-Folate and ^{177}Lu-IONPs only.

Energy Deposition and Dose Rate. The E_{dep} maps (Figure 3A) obtained as the output of GATE simulations for each radiotracer were used for the estimation of the 3D dose rate in the organs of mice at different time points. The 3D dose rates (Gy/h) were plotted as a function of time to generate dose rate curves for each radiotracer (Figure 3B).

Voxel-Based Absorbed Dose. The voxel-based absorbed dose (Gy/MBq) in the brain, heart wall, lungs, liver, and kidneys of normal mice obtained from ^{177}Lu-Folate, ^{177}Lu-IONPs, and ^{177}Lu-IONP-Folate are presented in Table 1. For ^{177}Lu-Folate, the absorbed dose was the highest in the kidneys (2.46 ± 0.50 Gy/MBq); however, ^{177}Lu-IONP-Folate and ^{177}Lu-IONPs delivered renal absorbed doses of 1.01 ± 0.17 and 0.52 ± 0.08 Gy/MBq, respectively. The absorbed dose in the liver was higher (1.09 ± 0.20 Gy/MBq) for ^{177}Lu-IONPs than for the other radiotracers. The absorbed dose to the kidneys from ^{177}Lu-IONP-Folate was 1.42 ± 0.48 Gy/MBq, less than that received from ^{177}Lu-Folate (Figure 4). The renal absorbed dose was reduced significantly when the IONP-based ^{177}Lu-labeled folate conjugate was used. The absorbed dose to the lungs was 0.75 ± 0.16 Gy/MBq higher with ^{177}Lu-IONP-Folate compared with that of ^{177}Lu-Folate.

The absorbed dose at the voxel level (Gy/MBq) in the brain, heart wall, lungs, liver, kidneys, and tumor of KB tumor bearing mice was also obtained from ^{177}Lu-Folate, ^{177}Lu-IONPs, and ^{177}Lu-IONP-Folate (Table 2). The voxel-based absorbed dose in the tumor was the highest with ^{177}Lu-IONP-Folate (0.37 ± 0.14 Gy/MBq) compared to the absorbed dose received by ^{177}Lu-Folate (0.29 ± 0.06 Gy/MBq) and ^{177}Lu-IONPs (0.21 ± 0.03 Gy/MBq). We found that the absorbed dose in the tumor was increased by 28 and 76% when the IONP-based ^{177}Lu-labeled folate conjugate was used compared to ^{177}Lu-Folate only and ^{177}Lu-IONPs, respectively. We observed that the renal absorbed dose in KB tumor bearing mice also reduced significantly with ^{177}Lu-IONP-Folate compared with ^{177}Lu-Folate.

Mean Absorbed Dose Estimation at Organ Level Using the MIRD Schema. We estimated the organ level mean absorbed dose (Gy/MBq) in the same organs due to all three radiotracers using the MIRD schema (Table 3). The absorbed doses estimated here are based on individualized activity distributions in the organs of a mouse; however, the *S*-values used in this study were estimated by Larsson et al.[28] from MOBY phantom.

We compared the voxel-based absorbed dose values obtained using GATE MC with the mean organ absorbed values measured using the MIRD schema (Figure 5A). We found voxel-based absorbed dose values were comparable to the organ level mean absorbed doses from ^{177}Lu-Folate and ^{177}Lu-IONPs. However, the absorbed dose in the organs estimated using the MIRD schema were slightly higher than the voxel-based absorbed dose received from ^{177}Lu-IONP-folate; the largest difference was 0.26 Gy/MBq, which was observed for the liver (Figure 5B).

DISCUSSION

We synthesized ^{177}Lu-labeled folate radiopharmaceutical conjugated with IONPs (^{177}Lu-IONP-Folate) and found that overall tissue distribution improved, and that the renal absorbed dose was reduced significantly. The SPECT image-based biodistribution results showed higher renal uptake of ^{177}Lu-Folate compared to ^{177}Lu-IONP-Folate. In contrast, ^{177}Lu-Folate showed lower uptake in the liver and blood compared to ^{177}Lu-IONP-Folate. In the same vein, voxel-based dosimetry revealed a reduced renal absorbed dose of ^{177}Lu-IONP-Folate.

Currently, various nanoparticles, including gold nanoparticles (AuNPs), IONPs, quantum dots, dendrimers, and micelles, have been utilized for in vivo molecular imaging and TRT.[29,30] Once nanoparticles are conjugated to therapeutic radioisotopes for tumor targeting, they are trapped in the tumor by both enhanced permeability and the retention (EPR) effect, and active targeting is achieved by binding appropriate ligands to the surface of nanoparticles.[31] Hector et al.[32] demonstrated a high retention of ^{177}Lu-DOTA-dendrimer-folate-bombesin with AuNPs in FRs and GRPRs overexpressed T47D breast cancer cells. In contrast, IONPs have a large surface area that provides a large number of functional groups for cross-linking to tumor-targeting ligands, such as peptides, for diagnostic imaging or targeted therapy.[30] Feng et al.[33] demonstrated that PEGylated IONPs of 10 nm exhibited relatively higher cellular uptake and tumor accumulation.

DOI: 10.1021/acs.molpharmaceut.8b01125
Mol. Pharmaceutics 2019, 16, 1498−1506

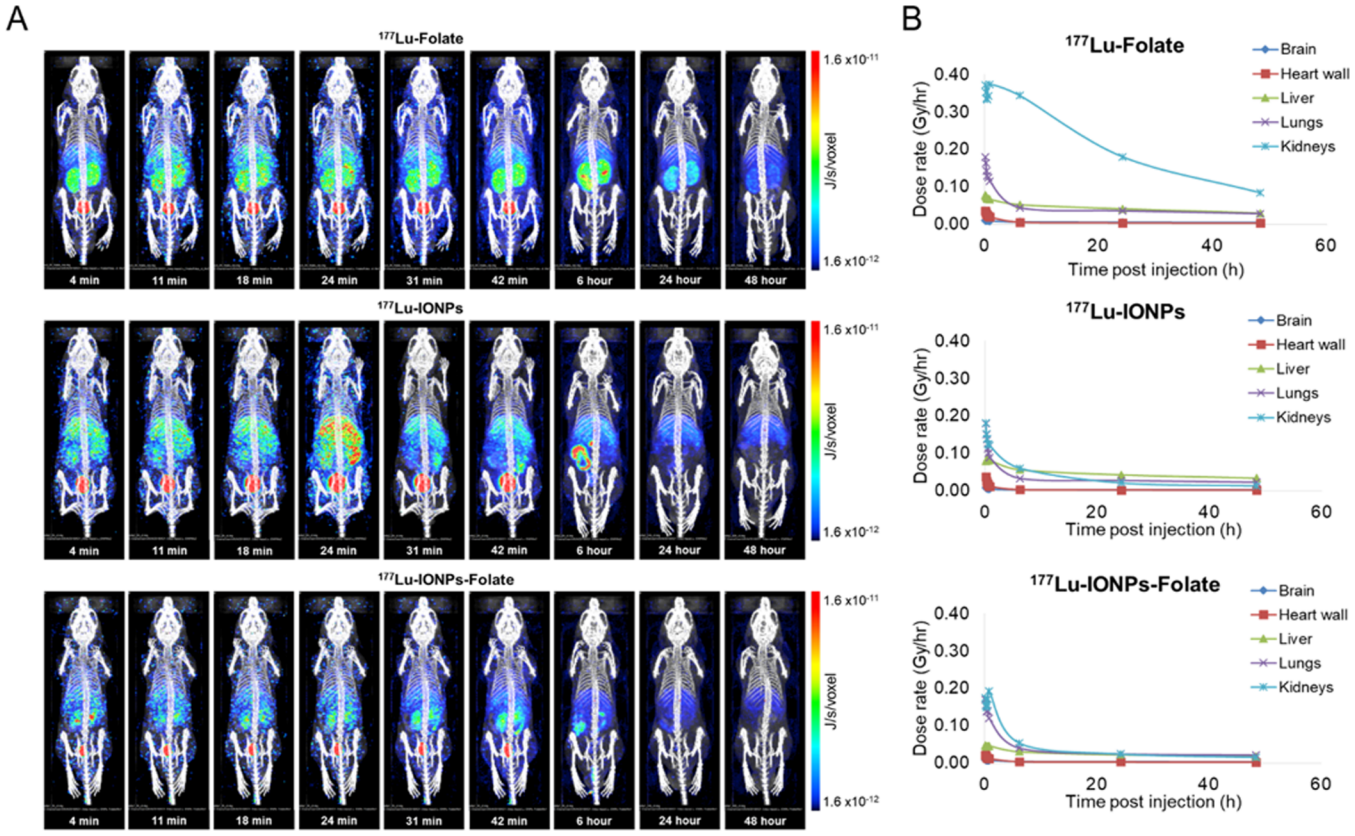

Figure 3. E_{dep} maps and dose rate curves of ^{177}Lu-Folate, ^{177}Lu-IONPs, and ^{177}Lu-IONP-Folate of normal mice. (A) MIP images showing E_{dep} maps overlaid on CT images of a mouse. (B) Dose-rate (mean, n = 5) as a function of time for different organs (brain, heart wall, liver, lungs, and kidneys; uncorrected for radiation decay). CT, computed tomography; IONPs, iron oxide nanoparticles; and MIP, maximum intensity projection.

Table 1. Voxel-Based Absorbed Dose (Mean ± SD[a]) Received by Organs of Normal Mice from ^{177}Lu-Folate, ^{177}Lu-IONPs, and ^{177}Lu-IONP-Folate

	voxel-based absorbed dose (Gy/MBq)		
organ	^{177}Lu-Folate	^{177}Lu-IONPs	^{177}Lu-IONP-Folate
brain	0.12 ± 0.01	0.08 ± 0.01	0.18 ± 0.02
heart wall	0.09 ± 0.01	0.08 ± 0.01	0.14 ± 0.01
lungs	0.73 ± 0.06	0.75 ± 0.10	1.20 ± 0.10
liver	0.76 ± 0.07	1.09 ± 0.20	0.96 ± 0.05
kidneys	2.46 ± 0.50	0.52 ± 0.08	1.01 ± 0.17

[a]SD, standard deviation.

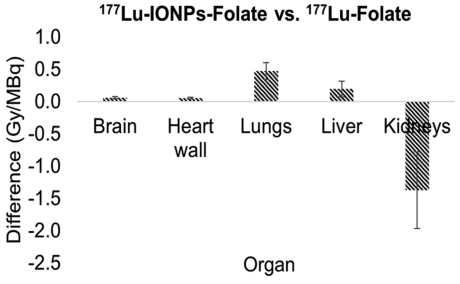

Figure 4. Difference in the voxel-based absorbed dose (mean ± SD) between ^{177}Lu-IONP-Folate and ^{177}Lu-Folate of normal mice. The absorbed dose was significantly reduced with ^{177}Lu-IONP-Folate. IONPs, iron oxide nanoparticles, and SD, standard deviation.

Table 2. Voxel-Based Absorbed Dose (Mean ± SD[a]) Received by Organs and Tumor from ^{177}Lu-Folate, ^{177}Lu-IONPs, and ^{177}Lu-IONP-Folate in KB Tumor Bearing Mice

	voxel-based absorbed dose (Gy/MBq)		
organ	^{177}Lu-Folate	^{177}Lu-IONPs	^{177}Lu-IONP-Folate
brain	0.12 ± 0.01	0.14 ± 0.01	0.12 ± 0.01
heart wall	0.10 ± 0.01	0.18 ± 0.01	0.22 ± 0.04
lungs	0.98 ± 0.11	1.25 ± 0.05	1.32 ± 0.23
liver	1.68 ± 0.22	2.24 ± 0.10	1.67 ± 0.30
kidneys	3.01 ± 0.63	0.88 ± 0.06	1.30 ± 0.24
tumor	0.29 ± 0.06	0.21 ± 0.03	0.37 ± 0.14

[a]SD, standard deviation.

Table 3. Mean Absorbed Dose at Organ Level (mean ± SD[a]) in Normal Mice from ^{177}Lu-Folate, ^{177}Lu-IONPs, and ^{177}Lu-IONP-Folate, Estimated Using the MIRD[a] Schema

	organ level absorbed dose (MIRD) (Gy/MBq)		
organ	^{177}Lu-Folate	^{177}Lu-IONPs	^{177}Lu-IONP-Folate
brain	0.12 ± 0.01	0.09 ± 0.01	0.24 ± 0.02
heart wall	0.07 ± 0.00	0.06 ± 0.01	0.14 ± 0.01
lungs	0.64 ± 0.03	0.61 ± 0.05	1.40 ± 0.13
liver	0.84 ± 0.10	1.29 ± 0.23	1.29 ± 0.05
kidneys	2.74 ± 0.37	0.54 ± 0.05	1.22 ± 0.21

[a]SD, standard deviation; MIRD, medical internal radiation dose.

A number of MC radiation transport codes (e.g., MCNP, EGSnrc, and Geant4) are widely available and implemented for preclinical voxel-based dosimetry either using the direct MC technique or by the estimation of murine *S*-values of different PET and SPECT radionuclides.[34−36] Recently, the

DOI: 10.1021/acs.molpharmaceut.8b01125
Mol. Pharmaceutics 2019, 16, 1498−1506

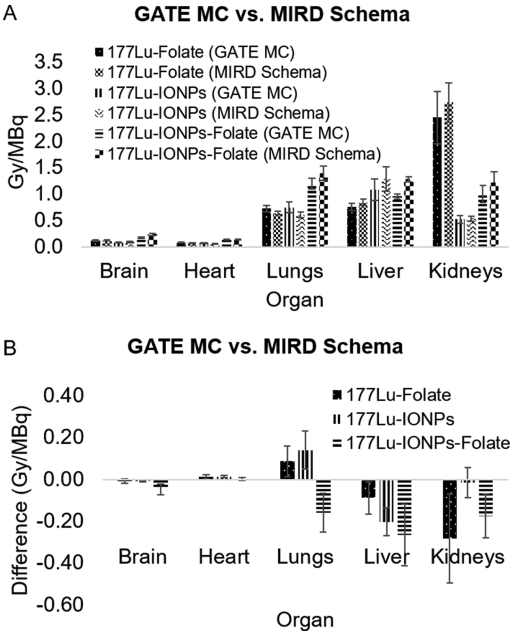

Figure 5. (A) Comparison of voxel-based absorbed dose (mean ± SD) estimated by GATE MC with mean absorbed dose at organ level (mean ± SD) calculated using the MIRD schema for ^{177}Lu-Folate, ^{177}Lu-IONPs, and ^{177}Lu-IONP-Folate in normal mice. (B) The difference between voxel-based absorbed dose (mean ± SD) estimated by GATE MC and mean absorbed dose at organ level (mean ± SD) measured using the MIRD schema for ^{177}Lu-Folate, ^{177}Lu-IONPs, and ^{177}Lu-IONP-Folate. GATE, Geant4 application for emission tomography; IONPs, iron oxide nanoparticles; MC, Monte Carlo; MIRD, medical internal radiation dose; and SD, standard deviation.

GATE MC simulation platform based on the Geant4 toolkit has been gaining its importance for voxel-based dosimetry application.[37−39] To the best of our knowledge, very few preclinical dosimetry studies have been performed using GATE MC.[40−43] All of these studies used the MOBY phantom that was developed by Segars et al.,[44] which is based on nonuniform rational B spline (NURBS) mathematical models. Kostou et al.[40] recently calculated the *S*-values of radioisotopes, including ^{177}Lu, with whole-body heterogeneous activity distributions as source organs in a MOBY phantom using the GATE MC simulation. As small variation in mice anatomy can result in significant differences in absorbed dose calculations, there could not be a specific mouse model with standardized organs and anatomy to implement dosimetry for murine studies.[21,40]

The voxel-based absorbed dose in kidneys delivered by ^{177}Lu-Folate was the highest; however, the absorbed dose decreased significantly with ^{177}Lu-IONP-Folate. Given the increased size of ^{177}Lu-IONP-Folate (>10 nm), the glomerular filtration rate decreased compared with ^{177}Lu-Folate, and hence, the radioactivity of ^{177}Lu-IONPs-Folate was retained in blood for a longer period.[45] Muller et al.[9] estimated the absorbed dose in tumor xenografts (1.80 Gy/MBq) and kidneys (3.44 Gy/MBq) of FR-positive KB tumor bearing mice using the MIRD schema. In our study, the voxel-based absorbed dose estimated in the kidneys of normal mice with ^{177}Lu-IONP-Folate was just 1.01 ± 0.17 Gy/MBq. We found that the total absorbed dose in the kidneys measured at voxel-level was 5.53 ± 0.94 Gy after the injection of 5.50 ± 0.10 MBq of ^{177}Lu-IONP-Folate. The maximum tolerated dose to the kidneys in TRT is 25 to 30 Gy,[46] which was almost 5 to 6 times higher than we obtained with ^{177}Lu-IONP-Folate in this study. Therefore, we can increase the activity of ^{177}Lu-IONP-Folate to be administered during the TRT of FR-positive tumor bearing mice to kill cancer cells more effectively without radiation nephropathy.

We compared the mean absorbed dose estimated using the MIRD schema with voxel-based absorbed dose measured using GATE MC for all three ^{177}Lu-radiotracers and found that the MIRD schema persistently overestimated the renal absorbed dose, although the differences were not significant. Parach et al.[47] compared the specific absorbed fraction values derived from GATE and the corresponding MIRD published data and found an acceptable agreement between the two results.

We also performed voxel-based dosimetry of ^{177}Lu-labeled conjugates in KB tumor bearing mice, where the absorbed dose in the tumor received by ^{177}Lu-IONPs-Folate was 28% higher than the absorbed dose received by ^{177}Lu-Folate only. We found that the absorbed doses to normal organs, such as lungs, liver, and kidneys, were higher than that of the tumor. According to the previous reports, the tolerable dose limit for the lungs, liver, and kidneys is 17.5, 30, and 25−30 Gy, respectively.[46,48] From the results obtained in our tumor dosimetry study, it can be observed that the lungs are a critical organ for ^{177}Lu-IONP-Folate TRT, and the maximum tolerable activity is 13.2 MBq (4.8 Gy to tumor). The absorbed dose received by the tumors in this manner seems to be low; however, it is known that the tumor cells are more sensitive to the radiation induced DNA damage than normal cells. Furthermore, the level of activity of radiotracers to be administered during TRT depends on the tolerable dose of the critical organ. A previous study performed on human cervical carcinoma cell lines (HeLa and SiHa) showed that the surviving fraction of the tumor cell was nearly 0.1 when the radiation dose of 5 Gy was given.[49] Therefore, in this study, we can achieve enough therapeutic effect to an extent, not exceeding the tolerable dose limit of normal organs.

The in vitro cell binding affinity of ^{177}Lu-Folate and ^{177}Lu-IONP-Folate was also measured in this study using FR-positive KB cells. Our studies suggest that the binding affinity of the prepared ^{177}Lu-IONP-Folate in mice bearing FR-overexpressed tumor xenografts was high compared with that of ^{177}Lu-Folate. This could be due to the multivalent ligand−receptor binding of the ^{177}Lu-IONPs-Folate, which occurs because the peptide−nanoparticle conjugate provides a surface for simultaneous interactions with the cell surface, giving rise to multivalent effects.[50]

Furthermore, the advantage of patient-specific voxel-based dosimetry is to predict biologic effect more effectively during targeted radionuclide therapy.[48] Dose-volume histograms (DVHs) can be obtained using the patient-specific 3-dimensional distributions of the absorbed dose within the target volume of the tumor, which is particularly useful because it could be the starting point for radiobiologic interpretation and modeling of the dose distribution for response assessment during cancer therapy.[51,52]

CONCLUSIONS

In conclusion, our results showed that the renal absorbed dose could be reduced to almost half with ^{177}Lu-IONP-Folate. We used SPECT/CT imaging data of real mice for MC simulation to show the variations in organ anatomy and activity

DOI: 10.1021/acs.molpharmaceut.8b01125
Mol. Pharmaceutics 2019, 16, 1498−1506

distribution to produce the individualized whole-body energy distribution for each mouse. Hence, we believe that our voxel-based absorbed doses calculated in the organs of mice from ^{177}Lu-Folate, ^{177}Lu-IONPs, and ^{177}Lu-IONP-Folate are highly accurate. This method could be applied during the TRT of FR-positive cancers for individualized dosimetry.

AUTHOR INFORMATION

Corresponding Authors

*Tel: +82-2-3668-8906; E-mail: wonza43@snu.ac.kr.

*Tel: +82-2-2072-2938; Fax: +82-2-745-2938; E-mail: jaes@snu.ac.kr.

ORCID

Jae M. Jeong: 0000-0003-2611-6020

Jae S. Lee: 0000-0001-7623-053X

Author Contributions

$^{\nabla}$A.G. and J.H.S. contributed to this work equally and are co-first authors.

Notes

The authors declare no competing financial interest.

ACKNOWLEDGMENTS

This work was supported by the National Research Foundation (NRF) funded by the Ministry of Science and ICT, Korea (Grant NRF-2017M3A9G5082640, NRF-2014M3C7034000, and NRF-2016R1A2B3014645).

REFERENCES

(1) Willmann, J. K.; van Bruggen, N.; Dinkelborg, L. M.; Gambhir, S. S. Molecular imaging in drug development. *Nat. Rev. Drug Discovery* **2008**, *7*, 591−607.

(2) Li, T.; Ao, E. C. I.; Lambert, B.; Brans, B.; Vandenberghe, S.; Mok, G. S. P. Quantitative imaging for targeted radionuclide therapy dosimetry - technical review. *Theranostics* **2017**, *7*, 4551−65.

(3) Dewaraja, Y. K.; Frey, E. C.; Sgouros, G.; Brill, A. B.; Roberson, P.; Zanzonico, P. B.; Ljungberg, M. MIRD Pamphlet No. 23: quantitative SPECT for patient-specific 3-dimensional dosimetry in internal radionuclide therapy. *J. Nucl. Med.* **2012**, *53*, 1310−1325.

(4) Pool, S. E.; Krenning, E. P.; Koning, G. A.; van Eijck, C. H. J.; Teunissen, J. J. M.; Kam, B.; Valkema, R.; Kwekkeboom, D. J.; de Jong, M. Preclinical and Clinical Studies of Peptide Receptor Radionuclide Therapy. *Semin. Nucl. Med.* **2010**, *40*, 209−218.

(5) Dash, A.; Chakraborty, S.; Pillai, M. R.; Knapp, F. F. Peptide receptor radionuclide therapy: an overview. *Cancer Biother.Radiopharm.* **2015**, *30*, 47−71.

(6) Ersahin, D.; Doddamane, I.; Cheng, D. Targeted radionuclide therapy. *Cancers* **2011**, *3*, 3838−55.

(7) Giblin, M. F.; Veerendra, B.; Smith, C. J. Radiometallation of receptor-specific peptides for diagnosis and treatment of human cancer. *In Vivo.* **2005**, *19*, 9−29.

(8) de Jong, M.; Breeman, W. A.; Kwekkeboom, D. J.; Valkema, R.; Krenning, E. P. Tumor Imaging and Therapy Using Radiolabeled Somatostatin Analogues. *Acc. Chem. Res.* **2009**, *42*, 873−80.

(9) Müller, C.; Struthers, H.; Winiger, C.; Zhernosekov, K.; Schibli, R. DOTA conjugate with an albumin-binding entity enables the first folic acid−targeted ^{177}Lu-radionuclide tumor therapy in mice. *J. Nucl. Med.* **2013**, *54*, 124−131.

(10) Shen, H.; Wang, L.; Chen, W.; Menard, K.; Hong, Y.; Tian, Y.; Bonacorsi, S. J.; Humphreys, W. G.; Lee, F. Y.; Gan, J. Tissue distribution and tumor uptake of folate receptor−targeted epothilone folate conjugate, BMS-753493, in CD2F1 mice after systemic administration. *Acta Pharm. Sin. B* **2016**, *6*, 460−467.

(11) Das, T.; Banerjee, S. Theranostic applications of Lutetium-177 in radionuclide therapy. *Curr. Radiopharm.* **2015**, *9*, 94−101.

(12) Birn, H.; Spiegelstein, O.; Christensen, E. I.; Finnell, R. H. Renal tubular reabsorption of folate mediated by folate binding protein 1. *J. Am. Soc. Nephrol.* **2005**, *16*, 608−15.

(13) Holm, J.; Hansen, S. I.; Høier-Madsen, M.; Bostad, L. A high-affinity folate binding protein in proximal tubule cells of human kidney. *Kidney Int.* **1992**, *41*, 50−5.

(14) Kolbert, K. S.; Watson, T.; Matei, C.; Xu, S.; Koutcher, J. A.; Sgouros, G. Murine S factors for liver, spleen, and kidney. *J. Nucl. Med.* **2003**, *44*, 784−791.

(15) Stabin, M. G.; Sparks, R. B.; Crowe, E. OLINDA/EXM: The second-generation personal computer software for internal dose assessment in nuclear medicine. *J. Nucl. Med.* **2005**, *46*, 1023−1027.

(16) Hippeläinen, E.; Tenhunen, M.; Sohlberg, A. Fast voxel-level dosimetry for (177)Lu labelled peptide treatments. *Phys. Med. Biol.* **2015**, *60*, 6685−700.

(17) Lee, M. S.; Kim, J. H.; Paeng, J. C.; Kang, K. W.; Jeong, J. M.; Lee, D. S.; Lee, J. S. Whole-body voxel-based personalized dosimetry: the multiple voxel S-value approach for heterogeneous media with nonuniform activity distributions. *J. Nucl. Med.* **2018**, *59*, 1133−1139.

(18) Dewaraja, Y. K.; Wilderman, S. J.; Ljungberg, M.; Koral, K. F.; Zasadny, K.; Kaminiski, M. S. Accurate Dosimetry in 131I Radionuclide Therapy Using Patient-Specific, 3-Dimensional Methods for SPECT Reconstruction and Absorbed Dose Calculation. *J. Nucl. Med.* **2005**, *46*, 840−849.

(19) Flynn, A. A.; Green, A. J.; Pedley, R. B.; Boxer, G. M.; Boden, R.; Begent, R. H. A mouse model for calculating the absorbed beta-particle dose from 131I- and 90Y-labeled immunoconjugates, including a method for dealing with heterogeneity in kidney and tumor. *Radiat. Res.* **2001**, *156*, 28−35.

(20) Dewaraja, Y. K.; Wilderman, S. J.; Koral, K. F.; Kaminski, M. S.; Avram, A. M. Use of integrated SPECT/CT imaging for tumor dosimetry in I-131 radioimmunotherapy: a pilot patient study. *Cancer Biother.Radiopharm.* **2009**, *24*, 417−26.

(21) Boutaleb, S.; Pouget, J. P.; Hindorf, C.; Pelegrin, A.; Barbet, J.; Kotzki, P.-O.; Bardies, M. Impact of mouse model on preclinical dosimetry in targeted radionuclide therapy. *Proc. IEEE* **2009**, *97*, 2076−2085.

(22) Moon, S. H.; Yang, B. Y.; Kim, Y. J.; Hong, M. K.; Lee, Y.-S.; Lee, D. S.; Chung, J.-K.; Jeong, J. M. Development of a complementary PET/MR dual-modal imaging probe for targeting prostate-specific membrane antigen (PSMA). *Nanomedicine* **2016**, *12*, 871−879.

(23) Kim, W. H.; Kim, C. G.; Kim, M. H.; et al. Preclinical evaluation of isostructural Tc-99m-and Re-188-folate-Gly-Gly-Cys-Glu for folate receptor-positive tumor targeting. *Ann. Nucl. Med.* **2016**, *30*, 369−379.

(24) Gupta, A.; Kim, K. Y.; Hwang, D.; Lee, M. S.; Lee, D. S.; Lee, J. S. Performance evaluation and quantitative accuracy of multipinhole nanoSPECT/CT scanner for theranostic Lu-177 imaging. *J. Korean Phys. Soc.* **2018**, *72*, 1379−86.

(25) Valentin, J. Basic anatomical and physiological data for use in radiological protection: reference values: ICRP Publication 89. *Ann. ICRP* **2002**, *32*, 1−277.

(26) Matsumoto, M.; Nishimura, T. Mersenne twister: a 623-dimensionally equidistributed uniform pseudo-random number generator ACM Trans. *Model Comput. Simul.* **1998**, *8*, 3−30.

(27) Sarrut, D.; Bardiès, M.; Boussion, N.; Freud, N.; Jan, S.; Létang, J. M. A review of the use and potential of the GATE Monte Carlo simulation code for radiation therapy and dosimetry applications. *Med. Phys.* **2014**, *41*, 064301.

(28) Larsson, E.; Strand, S. E.; Ljungberg, M.; Jönsson, B. A. Mouse S-factors based on Monte Carlo simulations in the anatomical realistic MOBY phantom for internal dosimetry. *Cancer Biother.Radiopharm.* **2007**, *22*, 438−42.

(29) Yang, L.; Peng, X. H.; Wang, Y. A.; et al. Receptor-targeted nanoparticles for In vivo imaging of breast cancer. *Clin. Cancer Res.* **2009**, *15*, 4722.

DOI: 10.1021/acs.molpharmaceut.8b01125
Mol. Pharmaceutics 2019, 16, 1498−1506

(30) Peng, X.; Qian, X.; Mao, H.; Wang, A.; Chen, Z.; Nie, S.; Shin, D. Targeted magnetic iron oxide nanoparticles for tumor imaging and therapy. *Int. J. Nanomed.* **2008**, *3*, 311−321.
(31) Lee, D. S.; Im, H. J.; Lee, Y. S. Radionanomedicine: Widened perspectives of molecular theragnosis. *Nanomedicine* **2015**, *11*, 795−810.
(32) Mendoza-Nava, H.; Ferro-Flores, G.; Ramirez, F. M.; et al. ^{177}Lu-dendrimer conjugated to folate and bombesin with gold nanoparticles in the dendritic cavity: a potential theranostic radiopharmaceutical. *J. Nanomater.* **2016**, *2016*, 1039258.
(33) Feng, Q.; Liu, Y.; Huang, J.; Chen, K.; Huang, J.; Xiao, K. Uptake, distribution, clearance, and toxicity of iron oxide nanoparticles with different sizes and coatings. *Sci. Rep.* **2018**, *8*, 2082.
(34) Visvikis, D.; Bardies, M.; Chiavassa, S.; Danford, C.; Kirov, A.; Lamare, F.; Maigne, L.; Staelens, S.; Taschereau, R. Use of the GATE Monte Carlo package for dosimetry applications. *Nucl. Instrum. Methods Phys. Res., Sect. A* **2006**, *569*, 335−340.
(35) Keenan, M. A.; Stabin, M. G.; Segars, W. P.; Fernald, M. J. RADAR realistic animal model series for dose assessment. *J. Nucl. Med.* **2010**, *51*, 471−6.
(36) Bitar, A.; Lisbona, A.; Bardiès, M. S-factor calculations for mouse models using Monte-Carlo simulations. *Q J. Nucl. Med. Mol. Imaging.* **2007**, *51*, 343−351.
(37) Jan, S.; Santin, G.; Strul, D.; et al. GATE: a simulation toolkit for PET and SPECT. *Phys. Med. Biol.* **2004**, *49*, 4543.
(38) Agostinelli, S.; Allison, J.; Amako, K.; et al. Geant4-a simulation toolkit. *Nucl. Instrum Methods Phys. Res. A* **2003**, *506*, 250−303.
(39) Jan, S.; Benoit, D.; Becheva, E.; et al. GATE V6: a major enhancement of the GATE simulation platform enabling modelling of CT and radiotherapy. *Phys. Med. Biol.* **2011**, *56*, 881−901.
(40) Kostou, T.; Papadimitroulas, P.; Loudos, G.; Kagadis, G. C. A preclinical simulated dataset of S-values and investigation of the impact of rescaled organ masses using the MOBY phantom. *Phys. Med. Biol.* **2016**, *61*, 2333−55.
(41) Mauxion, T.; Barbet, J.; Suhard, J.; Pouget, J. P.; Poirot, M.; Bardiès, M. Improved realism of hybrid mouse models may not be sufficient to generate reference dosimetric data. *Med. Phys.* **2013**, *40*, 052501.
(42) Taschereau, R.; Chatziioannou, A. F. Monte Carlo simulations of absorbed dose in a mouse phantom from 18-fluorine compounds. *Med. Phys.* **2007**, *34*, 1026−36.
(43) Perrot, Y.; Degoul, F.; Auzeloux, P.; et al. Internal dosimetry through GATE simulations of preclinical radiotherapy using a melanin-targeting ligand. *Phys. Med. Biol.* **2014**, *59*, 2183−2198.
(44) Segars, W. P.; Tsui, B. M.; Frey, E. C.; Johnson, G. A.; Berr, S. S. Development of a 4-D digital mouse phantom for molecular imaging research. *Mol. Imaging Biol.* **2004**, *6*, 149−59.
(45) Choi, H. S.; Liu, W.; Misra, P.; Tanaka, E.; Zimmer, J. P.; Itty Ipe, B.; Bawendi, M. G.; Frangioni, J. V. Renal Clearance of Nanoparticles. *Nat. Biotechnol.* **2007**, *25*, 1165−1170.
(46) Vilchis-Juárez, A.; Ferro-Flores, G.; Santos-Cuevas, C.; et al. Molecular targeting radiotherapy with cyclo-RGDfK(C) peptides conjugated to ^{177}Lu-labeled gold nanoparticles in tumor-bearing mice. *J. Biomed. Nanotechnol.* **2014**, *10*, 393−404.
(47) Parach, A. A.; Rajabi, H.; Askari, M. A. Assessment of MIRD data for internal dosimetry using the GATE Monte Carlo code. *Radiat. Environ. Biophys.* **2011**, *50*, 441−50.
(48) Emami, B.; Lyman, J.; Brown, A.; et al. Tolerance of normal tissue to therapeutic irradiation. *Int. J. Radiat Oncol Biol. Phys.* **1991**, *21*, 109−122.
(49) Bisht, K. S.; Bradbury, C. M.; Mattson, D.; et al. Geldanamycin and 17-allylamino-17-demethoxygeldanamycin potentiate the in vitro and in vivo radiation response of cervical tumor cells via the heat shock protein 90-mediated intracellular signaling and cytotoxicity. *Cancer Res.* **2003**, *63*, 8984−8995.
(50) Orocio-Rodríguez, E.; Ferro-Flores, G.; Santos-Cuevas, C. L.; Ramirez, F. d. M.; Ocampo-Garcia, B. E.; Azorin-Vega, E.; Sanchez-Garcia, F. M. Two novel nanosized radiolabeled analogues of somatostatin for neuroendocrine tumor imaging. *J. Nanosci. Nanotechnol.* **2015**, *15*, 4159−4169.
(51) Prideaux, A. R.; Song, H.; Hobbs, R. F.; He, B.; Frey, E. C.; Ladenson, P. W.; Wahl, R. L.; Sgouros, G. Three-dimensional radiobiologic dosimetry: application of radiobiologic modeling to patient-specific 3-dimensional imaging-based internal dosimetry. *J. Nucl. Med.* **2007**, *48*, 1008−1016.
(52) Sgouros, G.; Frey, E.; Wahl, R.; He, B.; Prideaux, A.; Hobbs, R. Three-dimensional imaging-based radiobiological dosimetry. *Semin. Nucl. Med.* **2008**, *38*, 321−24.

DOI: 10.1021/acs.molpharmaceut.8b01125
Mol. Pharmaceutics 2019, 16, 1498−1506